ADVANCED OPTICAL MATERIALS
www.advopticalmat.de

Strategies to Maximize the Dopant-To-Exciton Emission Ratio in Mn-Doped $CsPbCl_3$ Nanocrystals

Nadesh Fiuza-Maneiro, Iago López-Fernández, Junzhi Ye, Yunwei Zhang, Clara Otero-Martínez, Linjie Dai, Manuel Ceballos, Subarna Samanta, Pablo del Pino, Akshay Rao, Sergio Gómez-Graña,* Robert L. Z. Hoye, and Lakshminarayana Polavarapu**

Dedicated to Prof. Luis M Liz-Marzan on the occasion of his 60th birthday

Doping $CsPbCl_3$ perovskite nanocrystals (NCs) with Mn^{2+} has gained attention due to their interesting emission properties. However, the photoluminescence (PL) spectra of these NCs display both dopant and exciton emission peaks. It is critical to achieve color purity for light–emitting diode (LED) applications, but the factors that govern this remain unclear. Herein, a systematic investigation of the factors determining the exciton-to-dopant energy transfer process in Mn^{2+}-doped $CsPbCl_3$ NCs is presented to reveal how the exciton-to-Mn^{2+} emission ratio can be maximized. These findings indicate that this process is not only affected by dopant concentration and halide (Cl/Br) composition, but also by the co-dopants used, as well as surface passivation. These factors can potentially account for the discrepancies in the exciton-to-dopant emission ratios across the literature. These results show that post-synthetic surface passivation of Mn^{2+}-doped $CsPbCl_3$ NCs with quaternary ammonium salt, such as dimethyldidodecylammonium chloride (DDACl), drastically enhances the exciton-to-Mn^{2+} emission ratio, achieving a two-fold increase. Ultrafast pump-probe spectroscopy surprisingly reveals that the passivation can introduce shallow trap states that enhance energy transfer to dopant sites and influence overall luminescence efficiency through non-radiative decay processes. This study sets guidelines for maximizing dopant emission in doped perovskite NCs.

1. Introduction

Over the past decade, lead halide perovskite nanocrystals (LHP NCs) have been intensively explored due to their exceptional optoelectronic properties, including high photoluminescence quantum yields (PLQYs), tunable emission across the visible spectrum, high charge carrier diffusion, and facile synthesis compared to classical quantum dots.[1–5] Such attributes make LHP NCs highly promising candidates for a broad range of optoelectronic applications, including light–emitting diodes (LEDs), lasers, single photon generation, photovoltaic cells, photodetectors, and photocatalysis.[1,6–10] Halide perovskites generally exhibit an ABX_3 crystal structure, where A is a monovalent cation, typically Cs^+, MA^+, and FA^+, B is a divalent cation, usually Pb^{2+}, and X is a halide ion (Cl^-, Br^-, or I^-). It has been demonstrated that replacing a small amount of Pb^{2+} with specific metallic ions—such as alkaline

N. Fiuza-Maneiro, I. López-Fernández, C. Otero-Martínez[+], S. Samanta, S. Gómez-Graña, L. Polavarapu
CINBIO
Universidade de Vigo
Materials Chemistry and Physics Group
Department of Physical Chemistry
Campus Universitario Lagoas
Marcosende, Vigo 36310, Spain
E-mail: segomez@uvigo.gal; lakshmi@uvigo.es

The ORCID identification number(s) for the author(s) of this article can be found under https://doi.org/10.1002/adom.202502815

[+]Present address: Nanochemistry, Istituto Italiano di Tecnologia, Via Morego 30, 16163 Genova, Italy

© 2025 The Author(s). Advanced Optical Materials published by Wiley-VCH GmbH. This is an open access article under the terms of the Creative Commons Attribution License, which permits use, distribution and reproduction in any medium, provided the original work is properly cited.

DOI: 10.1002/adom.202502815

J. Ye, L. Dai, A. Rao
Cavendish Laboratory
University of Cambridge
Cambridge CB3 0HE, UK
E-mail: junzhi.ye@chem.ox.ac.uk

J. Ye, R. L. Z. Hoye
Inorganic Chemistry Laboratory
University of Oxford
South Parks Road, Oxford OX1 3QR, UK

Y. Zhang
School of Physics
Sun Yat-sen University
Guangzhou 510275, China

M. Ceballos, P. del Pino
Centro Singular de Investigación en Química Biolóxica e Materiais Moleculares (CiQUS)
Universidade de Santiago de Compostela
Santiago de Compostela 15782, Spain

-earth metal ions (Ba^{2+}, Sr^{2+}), transition metal ions (Mn^{2+}, Zn^{2+}, Cd^{2+}, and Ni^{2+}), and rare-earth or other trivalent ions (Al^{3+}, Fe^{3+}, Bi^{3+}) can dramatically improve the optoelectronic properties or induce new functionalities.[11–19] In particular, Mn^{2+}-doping/alloying has been shown to be effective in increasing the stability and intensity of photoluminescence (PL).[4,20–26] Similar to classical semiconductors, Mn^{2+}-doping/alloying in $CsPbCl_3$ results in the appearance of characteristic yellow-orange emission, attributed to non-radiative energy transfer that occurs from the excited host to the Mn^{2+}-dopant, which then relaxes radiatively via spin-forbidden $^4T_1 \rightarrow {}^6A_1$ transition (phosphorescence).[27–32] Despite the significant exploration of Mn^{2+}-doping in $CsPbCl_3$ NCs, there are discrepancies in the dopant-to-exciton emission ratios depending on the synthesis parameters.[1,33–42] The PL spectra of $CsPbCl_3$ NCs have shown that in some cases, excitonic peaks exhibit higher intensity than dopant emissions, while in other cases, the opposite trend is observed.[27,43–46] The presence of both excitonic and dopant emission peaks can be problematic for color-pure LEDs that often require a single peak. Mixed color emission reduces the sharpness and efficiency of LEDs. The presence of two peaks can be a sign of incomplete doping or inefficient energy transfer from the exciton to the dopant due to an energy level mismatch or other non-radiative channels. In addition, chloride-based perovskites are less defect-tolerant compared to their bromide and iodide counterparts.[47–49] The presence of deep traps in $CsPbCl_3$ NCs promotes non-radiative recombination, which not only lowers the quantum yield but also competes with the exciton-to-dopant energy transfer process, ultimately reducing dopant emission.[50] Moreover, recent reports have demonstrated significant advances in the practical applications of Mn-doped perovskite nanocrystals, highlighting their potential in optoelectronic devices and underscoring the relevance of further studies in this area.[51] Given the ionic nature of the surface capping ligands[52] and the formation of these deep traps, it is pertinent to explore a post-synthetic surface passivation strategy to mitigate surface trap states and enhance dopant emission.[53,54] Therefore, the parameters governing the exciton-to-dopant energy transfer and the optimization of dopant emission Mn^{2+}-doped $CsPbCl_3$ NCs are not well understood. This knowledge gap highlights the need for a systematic examination of the key parameters that govern the dopant-to-exciton (host) emission ratio, which is crucial for achieving emission color purity in doped semiconductor systems.

In this work, we report a systematic investigation of the factors that influence the dopant to exciton emission ratio in Mn^{2+}-doped $CsPbCl_3$ perovskite NCs, where the excited energy generated in host NCs transfers to the Mn^{2+} dopants, leading to an orange color emission. First, we studied the effect of Mn^{2+}-dopant concentration on the dopant-to-exciton ratio by varying the percentage of $MnCl_2$ precursor in the reaction medium during the $CsPbCl_3$ NCs synthesis. Then, the relation between the emission peak of the host NCs (*i.e.*, bandgap) and the Mn^{2+} dopant emission is investigated through reversible halide ion exchange (Cl→Br). Furthermore, the influence of the co-dopant (Mg^{2+}) and the post-synthetic surface passivation with quaternary ammonium salt (DDACl and DDABr) is investigated. We performed time-resolved photoluminescence and transient absorption spectroscopy of the doped nanocrystals to explore the origin of the significant enhancement of the dopant-to-exciton emission through surface passivation.

2. Results and Discussion

Pristine and Mn^{2+}-doped $CsPbCl_3$ perovskite NCs were synthesized via a high-temperature (≈180 °C) hot-injection method using oleylamine (OAm) and oleic acid (OA) ligands (**Figure 1a**). The Mn^{2+}-dopant concentration is varied by controlling the $PbCl_2$ and $MnCl_2$ precursor ratio in the reaction medium while their total concentration remains constant. The resulting pristine NCs exhibit a typical exciton luminescence at 400 nm, while the doped-NCs demonstrated dual photoluminescence with ≈400 nm excitonic emission from the $CsPbCl_3$ host and ≈600 nm emission attributed to Mn^{2+} (Figure 1b). The doped NCs exhibit typical cubic morphology with an average edge length of 10.6 ± 1.4 nm (Figure 1c; Figure S1, Supporting Information). The PL spectra of the doped NCs show that the peak intensity of the dopant emission increases relative to the exciton emission intensity with increasing Mn^{2+} precursor concentration in the reaction medium, reaching a maximum at 70%, after which it begins to decrease (Figure S2, Supporting Information). The ratio of the dopant to the exciton emission intensities with different Mn^{2+} precursor concentrations is depicted in **Figure 2d**. Notably, the maximum dopant-to-exciton emission ratio, indicating efficient energy transfer, was achieved with 70 mmol.% of $MnCl_2$ with respect to $PbCl_2$ in the precursor solution (Figure 2d; Table S1, Supporting Information). Interestingly, this result aligns with the optimum Mn^{2+} precursor concentration determined by machine learning-directed predictive models, which observed optimal energy transfer with 60% manganese precursor content.[55] The successful incorporation of Mn into the crystal structure was further confirmed through X-ray diffraction (XRD) analysis (Figure S3, Supporting Information). This was evidenced by a slight shift in peak positions toward higher diffraction angles, and this reduction in lattice parameter is consistent with the smaller ionic radius of Mn^{2+} compared to Pb^{2+}. It should be noted that the concentration of Mn that we mentioned in this manuscript is the precursor concentration, not the concentration of Mn incorporated in the NCs. Despite requiring more than twice the amount of manganese precursor relative to lead precursor to achieve maximum dopant emission, this ratio is not maintained in the final perovskite NCs. Analysis by Inductively Coupled Plasma Spectroscopy (ICP) and Energy Dispersive Spectroscopy (EDS) showed that, despite the precursor solution containing 70% manganese, the resulting material incorporated manganese atoms, accounting for only ≈7 at. % and 9 at. % of the total cations, respectively (Table S2, Supporting Information) (See Supporting Information for more detailed information about EDX and ICP analysis).

Next, we investigated how the variation in halide ion composition and the resulting changes in bandgap affect the dopant-to-exciton emission ratio by performing reversible halide exchange (Cl↔Br) on Mn^{2+}-doped $CsPbCl_3$ NCs (synthesized with 70% $MnCl_2$ precursor). The variation in halide (Cl/Br) composition changes the bandgap of the host matrix with respect to the Mn^{2+} energy levels, as depicted in Figure 2a. The as-prepared Mn^{2+}-doped- $CsPbCl_3$ NCs were purified and redispersed in toluene for reversible halide exchange by treating them first with $PbBr_2$,

© 2025 The Author(s). Advanced Optical Materials published by Wiley-VCH GmbH

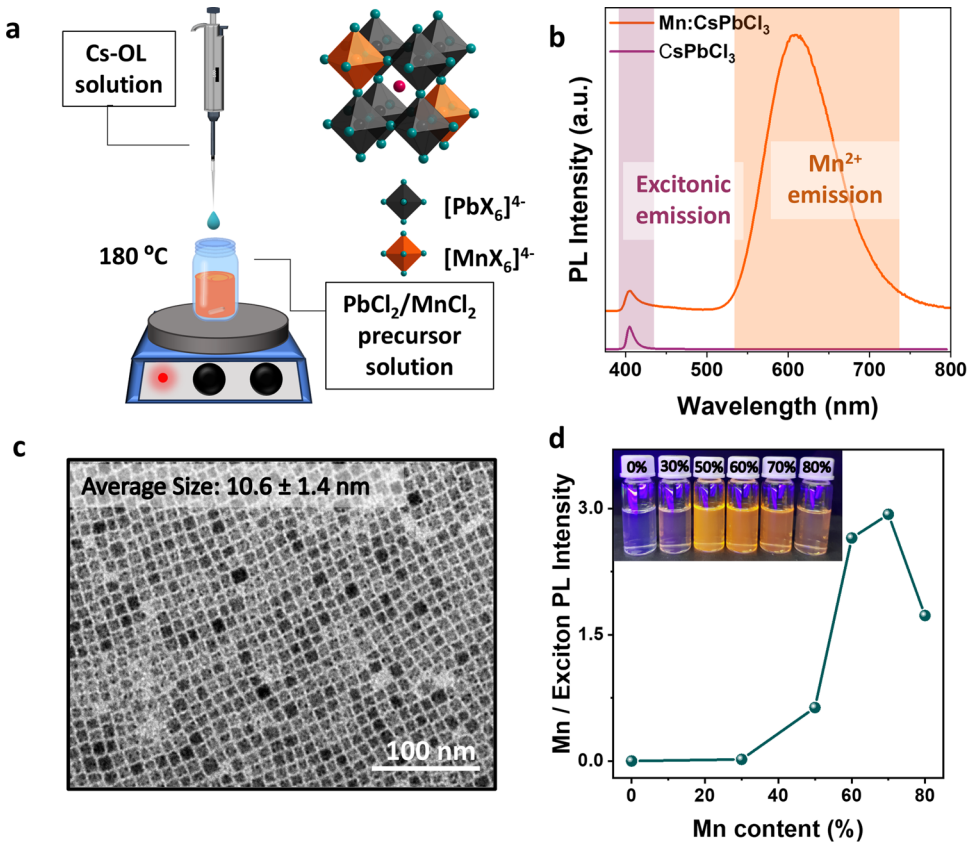

Figure 1. a) Schematic illustration of the hot-injection synthesis of Mn^{2+}-doped $CsPbCl_3$ NCs. b) PL spectrum of pristine and Mn-doped $CsPbCl_3$ NCs with 70% of $MnCl_2$ precursor. c) TEM image of Mn^{2+}-doped $CsPbCl_3$ NCs (70% of Mn^{2+}). d) Manganese dopant to exciton (host) emission ratio achieved with different Mn precursor ratios. The Mn/Exciton PL intensity is obtained by calculating the ratio between the integrated area of the Mn emission peak and the exciton emission peak.

then with $PbCl_2$ precursor solutions (see experimental section in Supporting Information for preparation of the precursor solution). The corresponding PL spectra of the two series of samples are shown in Figure 2b,c. First, the halide exchange (Cl→Br) was carried out by treating the Mn^{2+}-doped NCs with $PbBr_2$ solution. One can observe the obvious redshift of the exciton wavelength with increasing amounts of $PbBr_2$, due to the reduced bandgap caused by the replacement of Cl with Br in the crystal lattice. On the other hand, the peak intensity of the dopant emission initially increases relative to the exciton emission, but then decreases with further addition of $PbBr_2$ solution (Figure 2b). Importantly, the cation sublattice in these materials is structurally robust, so halide exchange proceeds almost exclusively through substitution of halide anions. Under these conditions, cation exchange is both kinetically and thermodynamically unfavorable, ensuring that Mn^{2+} remains stably incorporated at the B-site even when $PbBr_2$ is introduced as the halide source.[27] The initial increase in the Mn^{2+}-dopant emission upon replacing Cl with Br is attributed to the narrowing of the bandgap of the host lattice, leading to efficient energy transfer from the host to the Mn^{2+} ions (see the energy level diagram in Figure 2a). However, further increasing the Br content in the lattice causes the energy levels of the host to approach those of the dopants, resulting in back energy transfer, where the excited Mn^{2+} ion transfers its energy back to the host lattice instead of emitting light through radiative recombination. This process leads to a decrease in the dopant-to-exciton emission ratio due to further narrowing of the bandgap of the host lattice (Figure 2a).[34,37,55] In addition, we performed reverse anion exchange by treating the Mn^{2+}-doped $CsPb(Cl/Br)_3$ NCs with $PbCl_2$ and acquired their PL spectra (Figure 2c). The ratios of the exciton-to-dopant emission peaks for both cases are plotted in Figure 2d, and it shows that the maximum energy transfer coincides for both at a wavelength of 426 nm with the maximum ratio (Figure 2d). These results suggest that, to achieve maximum Mn^{2+} emission in doped perovskite NCs, the optimal synthesis conditions involve using ≈70% $MnCl_2$ precursor and tuning the Cl/Br halide composition to produce an excitonic emission peak ≈426 nm. Furthermore, we tested the effect of $PbCl_2$ treatment of the Mn^{2+}-doped $CsPbCl_3$ NCs, assuming that the filling of Cl vacancies on the surface leads to enhanced energy transfer; however, only a slight increase in the dopant emission was observed initially, but then decreased with further addition of $PbCl_2$ (Figure 2e). This is likely due to the inefficient surface passivation of $CsPbCl_3$ NCs with $PbCl_2$ precursor, as reported in our recent study.[18]

In general, surface defects in perovskite NCs, such as halide vacancies, undercoordinated Pb-ions, can act as nonradiative recombination centers.[50,56] These surface defects trap the exciton before it can reach the Mn^{2+} sites and thus reduce the energy transfer efficiency. Although narrow-gap iodide-based

© 2025 The Author(s). Advanced Optical Materials published by Wiley-VCH GmbH

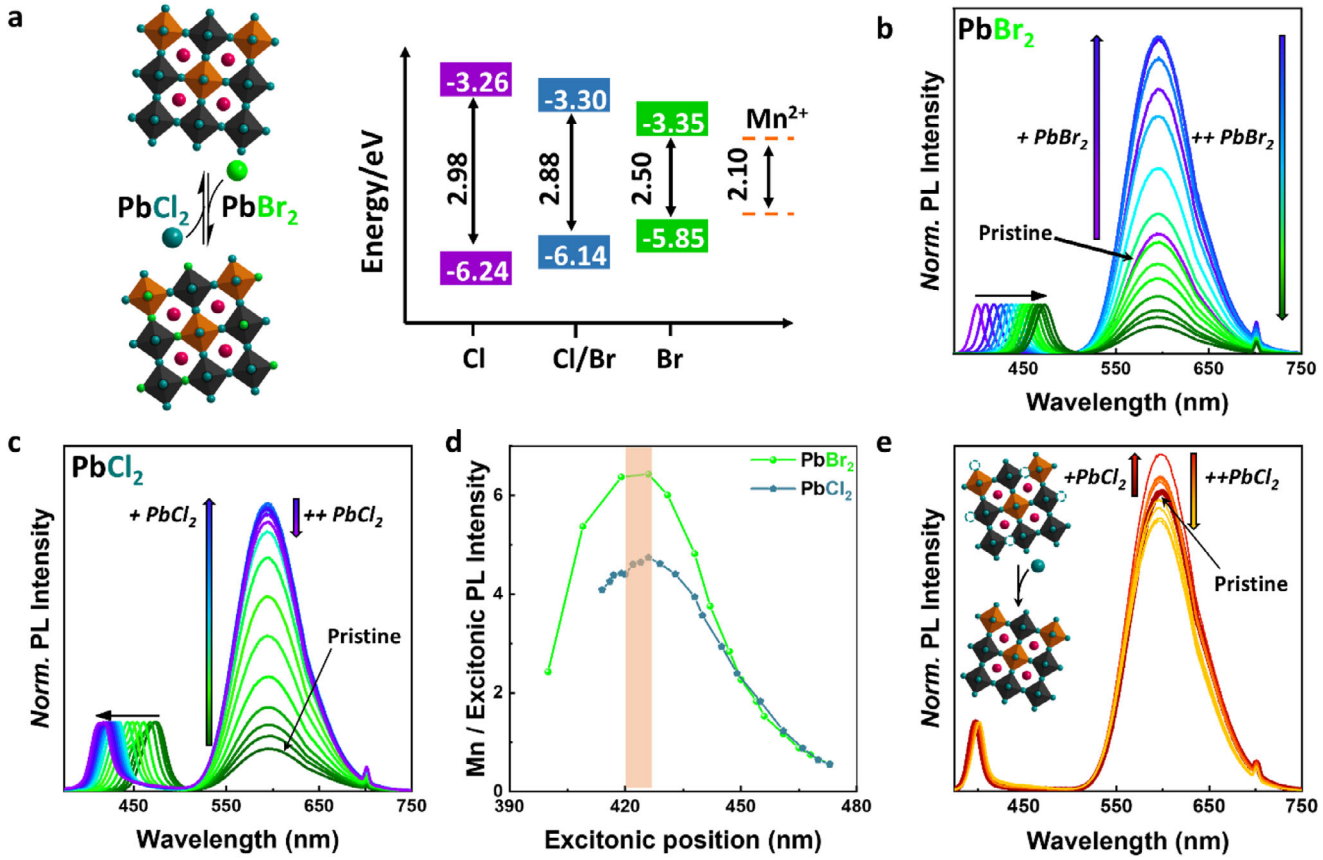

Figure 2. a) Scheme of anion exchange on Mn-doped $CsPbCl_3$ NCs. Band positions of $CsPbX_3$ and Mn^{2+} d-states. Adapted with permission from ref. [27]. b) Normalized PL spectra of Mn^{2+}-doped $CsPbCl_3$ NCs upon treating with different amounts of $PbBr_2$ precursor solution. The spectra are normalized to the exciton peak center. By adding low volumes of $PbBr_2$ (arrow from purple to dark blue), we can see a noticeable increase in the manganese emission, which decreases after reaching a maximum after adding more $PbBr_2$ solution (blue to green arrow). c) Normalized PL spectra of the samples obtained after reversible halide exchange by treating the Mn^{2+}-doped $CsPb(Cl/Br)_3$ NCs with $PbCl_2$ precursor solution. d) The ratio of Mn^{2+} -to-exciton emission intensities of the Mn^{2+}-doped-$CsPbCl_3$ NCs after reversible halide exchange with $PbBr_2$ and $PbCl_2$ precursor solutions (extracted from the spectra of Figure 2b,c). e) PL spectra of Mn^{2+}-doped-$CsPbCl_3$ NCs after treating them with different amounts of $PbCl_2$ precursor solution. First, a slight increase could be seen after adding $PbCl_2$ solution (dark red to red arrow), that decreases after reaching a maximum (red to yellow arrow).

perovskites are defect-tolerant, deep traps are more likely to form in chloride perovskites compared to their bromide and iodide counterparts due to their high ionic character and shorter Pb—Cl bond length.[18,50,57,58] In our recent study, we demonstrated that metal halides, such as $MgCl_2$, can effectively passivate the deep traps in $CsPbCl_3$ NCs, leading to enhanced photoluminescence.[18] Inspired by this work, we tested in situ passivation of Mn^{2+}-doped $CsPbCl_3$ NCs by $MgCl_2$, where extra $MgCl_2$ was added with $MnCl_2$ and $PbCl_2$ during synthesis. We selected 50% Mn-doping to see the effect of Mg^{2+} incorporation on the energy transfer efficiency. **Figure 3** shows the absorption and PL spectra of the Mn^{2+}-doped $CsPbCl_3$ and Mg^{2+}/Mn^{2+}-doped $CsPbCl_3$ colloidal NC solution (see experimental section for synthesis details). The Mg^{2+} incorporation leads to a blue shift in the absorption spectra due to its lower size compared to Pb and Mn. Interestingly, the PL spectra show that the dopant emission increased by sixfold relative to the exciton emission with in situ passivation with $MgCl_2$. The in situ passivation likely leads to the removal of deep traps, resulting in the enhanced energy transfer of excitons to Mn^{2+} dopants (see Figure S5, Supporting Information, for XRD data). XPS results confirmed that Mg was successfully incorporated into the structure, leading to a shift in its binding energies that demonstrates a different chemical environment (Figure S6, Supporting Information). In addition, ICP measurements confirmed the presence of Mg^{2+} atoms in the crystalline structure (Table S3, Supporting Information).

On the other hand, surface passivation can also be achieved with the ligands that can bind strongly to the NC surface. In perovskite NCs, the commonly used ligands, OAm and OA, are highly dynamic and prone to detachment from the surface, resulting in a high density of surface defects. In this regard, we used didodecyldimethyl ammonium bromide (DDABr), a ligand that can strongly bind to the perovskite NC surface for post-synthetic surface passivation of Mn^{2+}-doped $CsPbCl_3$ NCs. The DDABr ligand has been used as a dual-passivating agent to enhance the stability and luminescence efficiency, and can simultaneously replace cationic and anionic ligands from the NC surface.[56,59–61] The quaternary amines possess a strong affinity toward perovskite NC surface, partially substitute some of the OAm ligands, and fill halide vacancies at the surface.[56,59,62] In

© 2025 The Author(s). Advanced Optical Materials published by Wiley-VCH GmbH

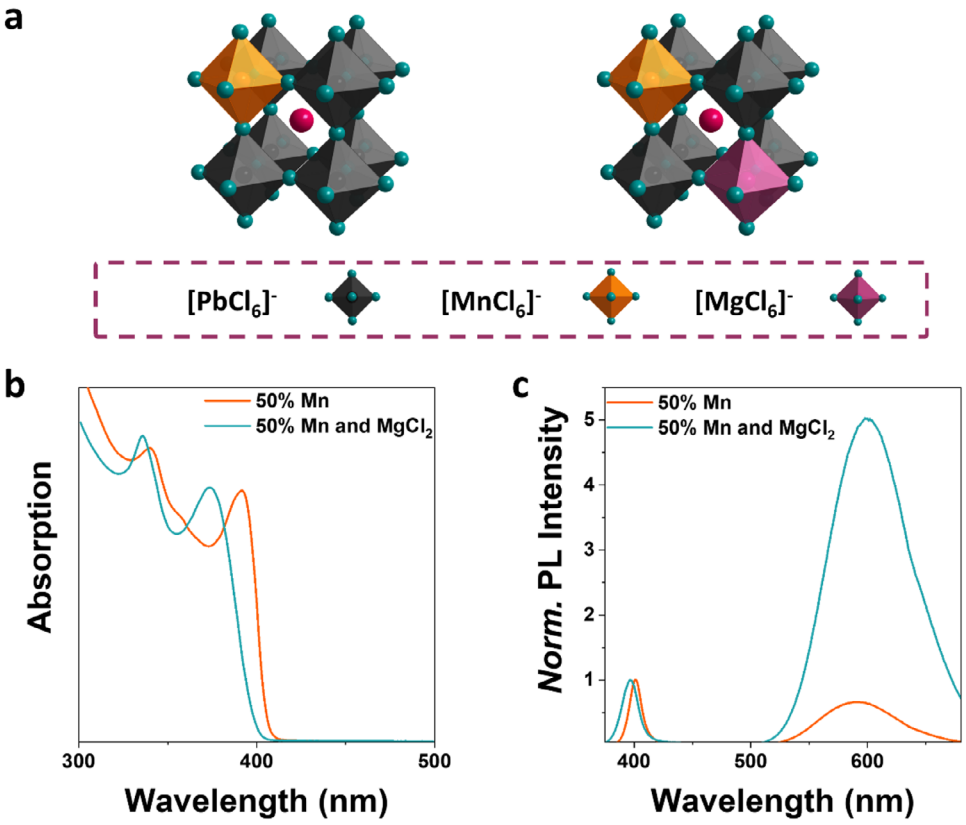

Figure 3. a) Representation of a possible example of the crystal structures observed in Mn-doped and Mn/Mg-doped $CsPbCl_3$ NCs. b,c) Normalized absorption and PL spectra of the corresponding NCs. The spectra are normalized at the absorption maximum and exciton PL, respectively.

addition, it can replace Cl ions with Br ions, resulting in the formation of Mn^{2+}-doped $CsPb(Cl/Br)_3$ NCs with a narrower bandgap. **Figure** 4b shows the normalized PL spectra of the doped-NCs before and after passivation with different amounts of DDABr solution. As expected, the excitonic emission peak red-shifts with increasing DDABr concentration due to halide exchange. Interestingly, the Mn^{2+} emission initially exhibits a drastic enhancement relative to the excitonic emission, but decreases with further addition of DDABr, similar to that of the $PbBr_2$ treatment (Figure 4b, and see Figure 2b,d for the PL spectra with $PbBr_2$ treatment). A plot of the ratios of Mn^{2+}/excitonic emission intensities versus the corresponding exciton peak positions shows a 17-fold sharp increase in the dopant emission relative to the excitonic emission at 415 nm (Figure 4c). The enhancement is higher than that achieved with $PbBr_2$ treatment, and the excitonic position at which the maximum energy transfer occurred is slightly blue-shifted. Therefore, these data show that the DDABr treatment enhances the exciton to dopant energy transfer not only through surface passivation but also by narrowing the bandgap via halide ion exchange. Subsequently, we proceeded to perform surface passivation with the analogous chlorine ligand-didodecyldimethyl ammonium chloride (DDACl). This procedure resulted in an observable increase in the ratio of Mn^{2+} to excitonic emission (Figure 4d). However, this enhancement was less pronounced compared to that achieved with $PbBr_2$ and DDABr treatments (Figure 4d,b), likely due to incomplete passivation and absence of band alignment, which have been shown to play a critical role in facilitating the efficient energy transfer of the exciton to dopants. Nevertheless, the enhancement is noteworthy given that the emission wavelength remains stable and unshifted, preserving the optical characteristics of the material. Figure 4e shows a gradual increase in dopant emission relative to the exciton as the added volume of DDACl increases. After reaching a maximum of two-fold enhancement, the ratio decreases, indicating saturation of the surface passivation. This saturation compromises the stability of the NCs as the ligand concentration in the medium continues to rise. Interestingly, the addition of DDACl initially enhances both exciton and manganese luminescence while maintaining a constant exciton-to-dopant emission ratio (Figure S7, Supporting Information). However, at higher DDACl concentrations, a decline in overall luminescence is observed, accompanied by an increase in the manganese-to-exciton emission ratio (Figure S7a,b, Supporting Information). Given that absorption remains largely unchanged compared to the pristine sample (Figure S7c, Supporting Information), this suggests the formation of shallow surface traps likely facilitates energy transfer, unlike the deep traps that prevent energy transfer.[63–65]

The modulation of charge-carrier dynamics upon passivation was systematically investigated by pump–probe transient absorption (TA) spectroscopy. As shown in Figure 5a (and Figure S8, Supporting Information), Mn^{2+}-doped $CsPbCl_3$ NCs exhibit shorter carrier lifetimes than pristine NCs, consistent with the dopant opening an additional host Mn energy-transfer pathway that competes with band-edge recombination. TA decays for the

© 2025 The Author(s). Advanced Optical Materials published by Wiley-VCH GmbH

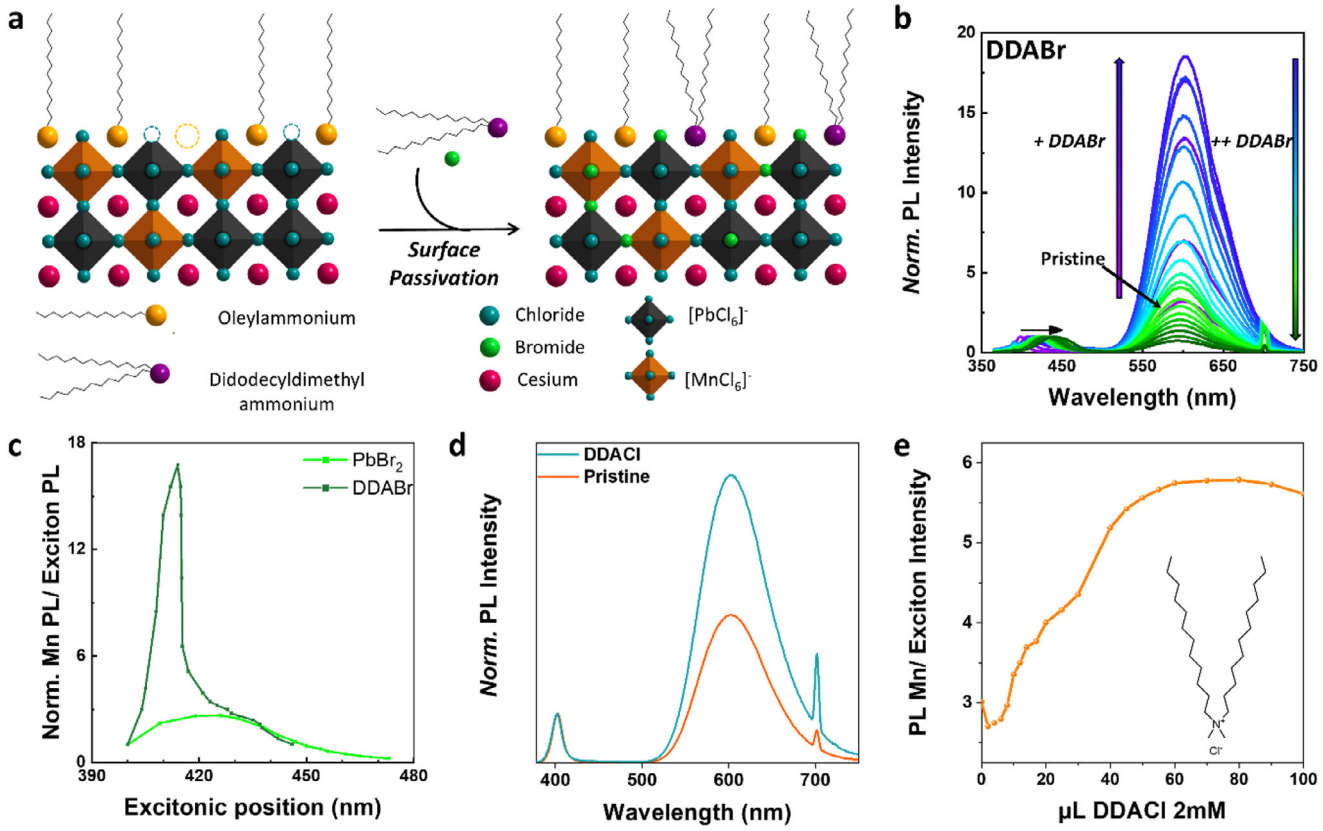

Figure 4. a) Schematic illustration of the surface passivation of Mn^{2+}-doped $CsPbCl_3$ NCs with didodecyldimethyl ammonium bromide (DDABr) ligand. Adapted with permission from ref. [59]. b) Normalized PL spectra of the doped-NCs with successive additions of DDABr (Normalized to the exciton). First, with low volume addition of DDABr, we can see an enhancement of dopant emission (arrow from purple to dark blue color), followed by a decrease of Mn^{2+} emission intensity after adding even more DDABr into the solution (dark blue to green arrow) c) A plot of the ratios of Mn^{2+} / Excitonic emission peak intensities relative to the excitonic emission position after passivation with $PbBr_2$ and DDABr. d) Normalized PL spectra of doped-NCs before and after passivation with DDACl (Normalized to the exciton). e) A plot of the ratios of Mn / Exciton PL Intensities versus different volumes of DDACl.

doped samples are well described by a bi-exponential model (τ_1, τ_2), in which we attribute τ_1 to indicate host to Mn transfer and τ_2 to band-edge recombination of the perovskite bleach. Passivation with DDACl produces a modest extension of the apparent lifetime in the Mn-doped NCs (Figure 5b), but, crucially, the fluence dependence reveals two distinct defect channels. In the untreated doped NCs, both τ_1 and τ_2 increased with pump fluence, indicating trap filling in the pristine material. After DDACl treatment, the behavior becomes selective: τ_1 still increases with fluence, whereas τ_2 decreases, implying that passivation suppresses deep, fast loss channels that influence the early, τ_1 component,[18] while introducing shallow, long-lived states that impact τ_2. At high fluence, differences between treated and untreated traces diminish as both defect populations approach saturation (see Figure S10a,b, Supporting Information). The same signature is clearer in pure $CsPbCl_3$ controls (Figure S10c,d, Supporting Information): the DDACl-treated trace decays more slowly at early times (before ~10 ns) but faster at late times (after ~10 ns) than the untreated trace, consistent with reduced deep-trap capture together with a higher density of shallow surface states after ligand exchange. While we do not measure trap energies directly, this interpretation aligns with DFT studies of $CsPbCl_3$, which show that V_{Cs} and V_{Cl} can yield both deep (0.77–1.02 eV) and shallow (≈0.14 eV) states depending on local coordination as shown in Figure S11 (Supporting Information).[47,66] This mixed outcome explains the reduction of host PL after DDACl (while the Mn/host ratio increases): deep traps are mitigated, but shallow states more efficiently funnel carriers to Mn, diminishing host emission (mechanism summarized in Figure 5d).[67,68] The TCSPC measurements of Mn emission (centered near 600 nm) show a longer emissive lifetime after passivation (Figure 5c; Figure S9, Supporting Information), confirming that energy transfer proceeds through the emissive channel and that DDACl suppresses nonradiative recombination from deep traps while enhancing shallow-trap-assisted transfer to the dopant.[63–65]

In summary, the dopant and exciton emission ratio or the exciton to dopant energy transfer depends on three factors, 1) the bandgap of the host materials (i.e., the alignment of host material conduction band to dopant energy), 2) the presence of the deep traps which suppresses energy transfer, and 3) the presence of shallow traps which facilitates energy transfer to dopants. The halide exchange studies show that the red-shifted exciton position aligns more closely with the Mn $^4T_1$ states, which leads to enhanced energy transfer with higher emission from Mn. The introduction of DDACl reshapes charge-carrier pathways by

© 2025 The Author(s). Advanced Optical Materials published by Wiley-VCH GmbH

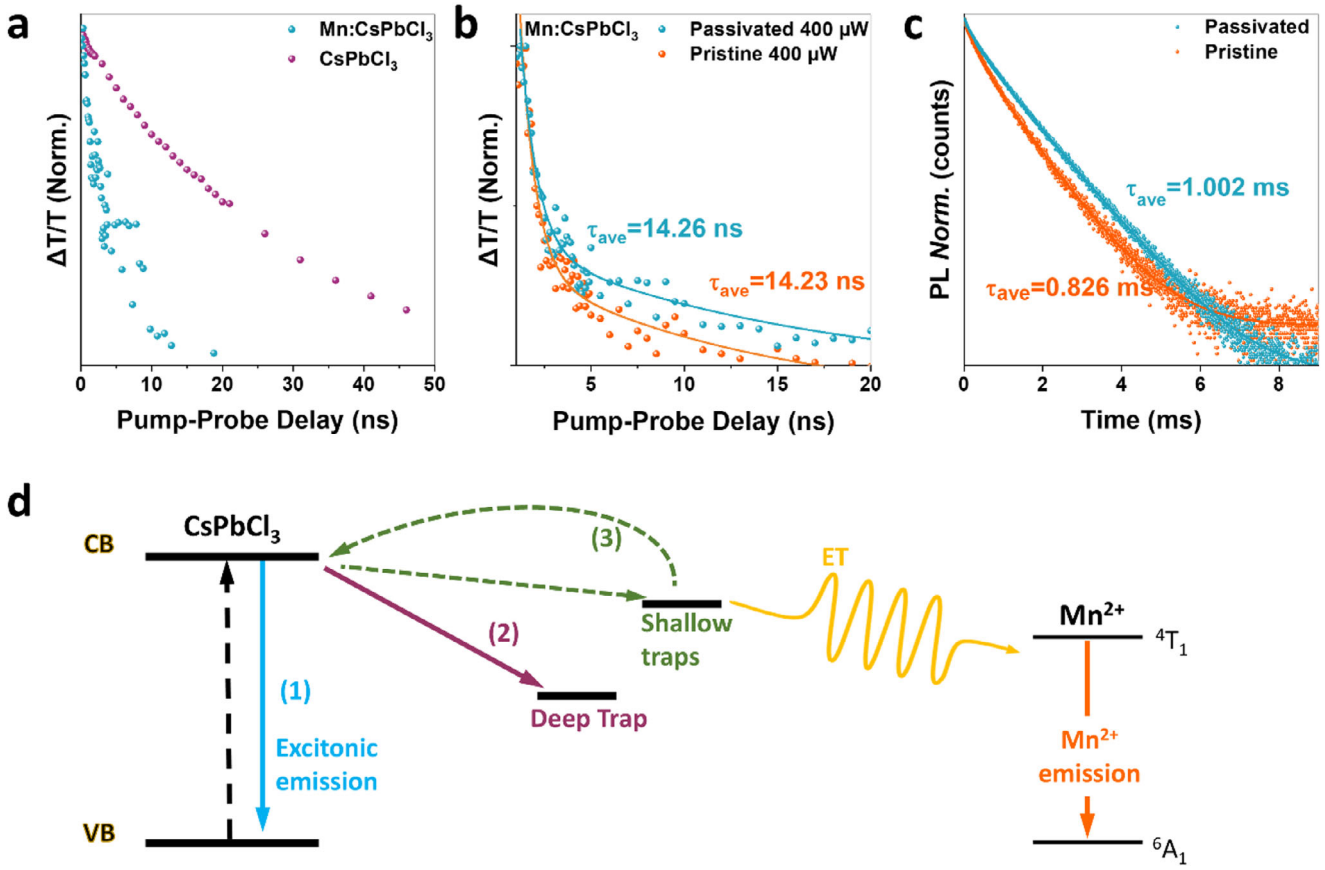

Figure 5. a) Transient absorption data for $CsPbCl_3$ and Mn-doped perovskite NCs. b) Transient absorption lifetime measurements for pristine and passivated with DDACl Mn-doped NCs. The pump used is 355 nm with a power of 400 μW, and the decay curve is probed at 390–395 nm to reveal the exciton decay. c) TCSPC measurements for pristine and passivated with DDACl Mn-doped NCs. The emission wavelength for the PL decay is at 600 nm. d) Scheme of the energy levels and electronic transitions in Mn-doped NCs. The pathway (1) is the excitonic emission from $CsPbCl_3$ NCs. Pathway (2) is the non-radiative recombination caused by deep-level traps, which usually correspond to the faster decay component, and these can be passivated by DDACl. Pathway (3) is the non-radiative recombination caused by surface shallow traps, which correspond to the slower, longer decay component, and these traps are introduced by the addition of excess DDACl. The shallow traps could facilitate charge transfer from CB to Mn by providing a competing pathway to (1).

suppressing the deep traps (Pathway 2) while enhancing the formation of shallow traps (Pathway 3), as can be observed in Figure 5d. The formation of these shallow traps leads to two key effects: (a) a decrease in overall perovskite photoluminescence intensity and (b) an increase in Mn-related emission. The mechanism behind this is that shallow trap states capture more charge-carriers, reducing the likelihood of deep trap recombination or perovskite emission. Consequently, while total PL intensity decreases, the relative contribution of Mn emission increases, enhancing dopant-related luminescence, and thus the dopant-to-exciton emission ratio.[63,65]

3. Conclusion

This study explores different strategies to enhance the dopant-to-exciton emission ratio in Mn^{2+}-doped $CsPbCl_3$ NCs. We demonstrate that dopant concentration, halide composition-dependent bandgap, co-doping, and surface passivation synergistically dictate the efficiency of exciton-to-Mn^{2+} energy transfer. In particular, band alignment exciton controllable by Br/Cl composition emerges as the dominant factor maximizing the dopant-to-exciton emission ratio, while co-dopants such as Mg^{2+} (in the form of $MgCl_2$ salt) enhance energy transfer by stabilizing the local lattice environment and halide passivation. Post-synthetic treatment with quaternary ammonium salts, such as DDACl, further promotes Mn^{2+} emission by modulating surface states, with ultrafast spectroscopy revealing that shallow trap states introduced during passivation can facilitate energy transfer. Overall, these insights establish a clear mechanistic framework for tuning dopant and exciton emission in Mn^{2+}-doped $CsPbCl_3$ NCs and provide a general strategy for optimizing luminescence in other doped semiconductor nanocrystals, advancing their design for high-performance optoelectronic applications.

Supporting Information

Supporting Information is available from the Wiley Online Library or from the author.

© 2025 The Author(s). Advanced Optical Materials published by Wiley-VCH GmbH

Acknowledgements

This work has received funding from the Spanish Agencia Estatal de Investigación (AEI/MCIN) through grants: L.P. acknowledges support from the Spanish Ministerio de Ciencia e Innovación through Ramón y Cajal grant (grant no. RYC2018-026103-I), EIC PATHFINDER CHALLEGNES project 101162112 (RADIANT), and a grant from Xunta de Galicia/ERDF (grant no. ED431f2021/05). S.G.-G. and L.P. acknowledge the support from MICIU/AEI/10.13039/501100011033 and ERDF/EU (grant nos. PID2023-147567NB-I00, TED2021-131628A-I00, and CNS2022-135531). J.Y. and R.L.Z.H. acknowledge funding from UK Research and Innovation for a Frontier Grant (no. EP/X0029900/1), awarded via the 2021 European Research Council Starting Grant scheme. They also thank St. John's College, Oxford, for financial support through a Welcome Grant and Large Grant, as well as support from the John Fell/Oxford University Press Research Fund. Y.W. Zhang acknowledges funding from the National Key R&D Program of China No. 2023YFA1610000, National Natural Science Foundation of China under Grant No.12304036, and the Guangdong Basic and Applied Basic Research Foundation (2023A1515010071). Funding for open access by the Universidade de Vigo/CISUG.

Conflict of Interest

The authors declare no conflict of interest.

Data Availability Statement

The data that support the findings of this study are available from the corresponding author upon reasonable request.

Keywords

$CsPbX_3$, energy transfer, halide perovskite nanocrystals, Mn^{2+} doping, post-synthetic surface passivation

Received: August 26, 2025
Revised: October 28, 2025
Published online:

[1] A. Dey, J. Ye, A. De, E. Debroye, S. K. Ha, E. Bladt, A. S. Kshirsagar, Z. Wang, J. Yin, Y. Wang, L. N. Quan, F. Yan, M. Gao, X. Li, J. Shamsi, T. Debnath, M. Cao, M. A. Scheel, S. Kumar, J. A. Steele, M. Gerhard, L. Chouhan, K. Xu, X. G. Wu, Y. Li, Y. Zhang, A. Dutta, C. Han, I. Vincon, A. L. Rogach, et al., *ACS Nano* **2021**, *15*, 10775.
[2] M. M. Byranvand, C. Otero-Martínez, J. Ye, W. Zuo, L. Manna, M. Saliba, R. L. Z. Hoye, L. Polavarapu, *Adv. Opt. Mater.* **2022**, *10*, 2200423.
[3] C. Otero-Martínez, J. Ye, J. Sung, I. Pastoriza-Santos, J. Pérez-Juste, Z. Xia, A. Rao, R. L. Z. Hoye, L. Polavarapu, *Adv. Mater.* **2022**, *34*, 2107105.
[4] A. K. Guria, S. K. Dutta, S. D. Adhikari, N. Pradhan, *ACS Energy Lett.* **2017**, *2*, 1014.
[5] S. Wang, W. Jiang, W. Cui, W. Jiang, M. Zhao, J. Sun, B. Liu, X. Lai, K. Shi, K. Pan, *Adv. Opt. Mater.* **2023**, *11*, 2202745.
[6] Z. Chen, R. L. Z. Hoye, H.-L. Yip, N. Fiuza-Maneiro, I. López-Fernández, C. Otero-Martínez, L. Polavarapu, N. Mondal, A. Mirabelli, M. Anaya, S. D. Stranks, H. Liu, G. Shi, Z. Xiao, N. Kim, Y. Kim, B. Shin, J. Shi, M. Liu, Q. Zhang, Z. Fan, J. C. Loy, L. Zhao, B. P. Rand, H. Arfin, S. Saikia, A. Nag, C. Zou, L. Y. Lin, H. Xiang, et al., *J. Phys.: Photonics* **2024**, *6*, 032501.
[7] J. S. Manser, J. A. Christians, P. V. Kamat, *Chem. Rev.* **2016**, *116*, 12956.
[8] E. P. Yao, Z. Yang, L. Meng, P. Sun, S. Dong, Y. Yang, Y. Yang, *Adv. Mater.* **2017**, *29*, 1606859.
[9] S. Rakshit, P. Piatkowski, I. Mora-Seró, A. Douhal, *Adv. Opt. Mater.* **2022**, *10*, 2102566.
[10] S. A. Veldhuis, P. P. Boix, N. Yantara, M. Li, T. C. Sum, N. Mathews, S. G. Mhaisalkar, *Adv. Mater.* **2016**, *28*, 6804.
[11] V. Naresh, N. Lee, *ACS Appl. Nano Mater* **2020**, *3*, 7621.
[12] W. H. Jeong, Z. Yu, L. Gregori, J. Yang, S. R. Ha, J. W. Jang, H. Song, J. H. Park, E. D. Jung, M. H. Song, S. H. Park, H. J. Snaith, A. Boretti, F. D. Angelis, D. Meggiolaro, J. Lee, H. Choi, B. R. Lee, *J. Mater. Chem. A* **2021**, *9*, 26750.
[13] M. Lu, X. Zhang, Y. Zhang, J. Guo, X. Shen, W. W. Yu, A. L. Rogach, *Adv. Mater.* **2018**, *30*, 1804691.
[14] K. Xing, X. Yuan, Y. Wang, J. Li, Y. Wang, Y. Fan, L. Yuan, K. Li, Z. Wu, H. Li, J. Zhao, *J. Phys. Chem. Lett.* **2019**, *10*, 4177.
[15] S. Thawarkar, P. J. S. Rana, R. Narayan, S. P. Singh, *Langmuir* **2019**, *35*, 17150.
[16] H. Kim, S. R. Bae, T. H. Lee, H. Lee, H. Kang, S. Park, H. W. Jang, S. Y. Kim, *Adv. Funct. Mater.* **2021**, *31*, 2102770.
[17] J. Li, X. Wang, Y. Tan, D. Liang, Y. Zou, L. Cai, T. Wu, K. Wen, Y. Wang, Y. Li, T. Song, L. Wang, B. Sun, *Adv. Opt. Mater.* **2020**, *8*, 2001073.
[18] N. Fiuza-Maneiro, J. Ye, S. K. Sharma, S. Chakraborty, S. Gómez-Graña, R. L. Z. Hoye, L. Polavarapu, *ACS Energy Lett.* **2025**, *10*, 1623.
[19] I. López-Fernández, D. Valli, C.-Y. Wang, S. Samanta, T. Okamoto, Y.-T. Huang, K. Sun, Y. Liu, V. S. Chirvony, A. Patra, J. Zito, L. De Trizio, D. Gaur, H.-T. Sun, Z. Xia, X. Li, H. Zeng, I. Mora-Seró, N. Pradhan, J. P. Martínez-Pastor, P. Müller-Buschbaum, V. Biju, T. Debnath, M. Saliba, E. Debroye, R. L. Z. Hoye, I. Infante, L. Manna, L. Polavarapu, *Adv. Funct. Mater.* **2024**, *34*, 2307896.
[20] D. Parobek, B. J. Roman, Y. Dong, H. Jin, E. Lee, M. Sheldon, D. H. Son, *Nano Lett.* **2016**, *16*, 7376.
[21] D. Rossi, D. Parobek, Y. Dong, D. H. Son, *J. Phys. Chem. C* **2017**, *121*, 17143.
[22] D. Parobek, Y. Dong, T. Qiao, D. H. Son, *Chem. Mater.* **2018**, *30*, 2939.
[23] C. H. A. Li, P. Geng, S. B. Shivarudraiah, M. Ng, X.-F. Zhang, B. Xu, L. Guo, J. E. Halpert, *Adv. Opt. Mater.* **2021**, *9*, 2100860.
[24] S. Das Adhikari, A. K. Guria, N. Pradhan, *J. Phys. Chem. Lett.* **2019**, *10*, 2250.
[25] A. N. Yadav, S. W. Jang, T. Samanta, J. M. Seo, J. H. Han, N. S. M. Viswanath, Y. M. Park, W. B. Im, *Adv. Opt. Mater.* **2024**, *12*, 2401460.
[26] G. Liu, S. Zhang, Y. Liu, F. Xuan, B. Teng, S. Ji, *Adv. Opt. Mater.* **2025**, *13*, 2402858.
[27] A. K. Guria, S. K. Dutta, S. D. Adhikari, N. Pradhan, *ACS Energy Lett.* **2017**, *2*, 1014.
[28] D. Ricciarelli, E. Mosconi, B. Merabet, O. Bizzarri, F. De Angelis, *J. Phys. Chem. Lett.* **2020**, *11*, 5482.
[29] A. Panigrahi, L. Mishra, P. Dubey, S. Dutta, S. Mondal, M. K. Sarangi, *J. Chem. Phys.* **2024**, *160*, 144709.
[30] K. R. Pradeep, R. Viswanatha, *APL Mater.* **2020**, *8*, 020901.
[31] W. Liu, Q. Lin, H. Li, K. Wu, I. Robel, J. M. Pietryga, V. I. Klimov, *J. Am. Chem. Soc.* **2016**, *138*, 14954.
[32] C. C. Lin, K. Y. Xu, D. Wang, A. Meijerink, *Sci. Rep.* **2017**, *7*, 45906.
[33] W. Xu, F. Li, F. Lin, Y. Chen, Z. Cai, Y. Wang, X. Chen, *Adv. Opt. Mater.* **2017**, *5*, 1700520.
[34] S. Paul, E. Bladt, A. F. Richter, M. Döblinger, Y. Tong, H. Huang, A. Dey, S. Bals, T. Debnath, L. Polavarapu, J. Feldmann, *Angew. Chem., Int. Ed.* **2020**, *59*, 6794.
[35] B. Su, M. S. Molokeev, Z. Xia, *J. Phys. Chem. Lett.* **2020**, *11*, 2510.
[36] D. Parobek, B. J. Roman, Y. Dong, H. Jin, E. Lee, M. Sheldon, D. H. Son, *Nano Lett.* **2016**, *16*, 7376.
[37] K. Xu, A. Meijerink, *Chem. Mater.* **2018**, *30*, 5346.
[38] S. Das Adhikari, A. K. Guria, N. Pradhan, *J. Phys. Chem. Lett.* **2019**, *10*, 2250.

© 2025 The Author(s). Advanced Optical Materials published by Wiley-VCH GmbH

[39] T. Qiao, D. Parobek, Y. Dong, E. Ha, D. H. Son, *Nanoscale* **2019**, *11*, 5247.
[40] K. Xu, J. F. Vliem, A. Meijerink, *J. Phys. Chem. C* **2019**, *123*, 979.
[41] W. J. Mir, M. Jagadeeswararao, S. Das, A. Nag, *ACS Energy Lett.* **2017**, *2*, 537.
[42] A. Chemmangat, S. Murray, P. V. Kamat, *J. Am. Chem. Soc.* **2025**, *147*, 4541.
[43] Y. Zhao, C. Xie, Y. Song, P. Yang, *J. Nanopart. Res.* **2020**, *22*, 147.
[44] S. Das Adhikari, S. K. Dutta, A. Dutta, A. K. Guria, N. Pradhan, *Angew. Chem., Int. Ed.* **2017**, *56*, 8746.
[45] B. Luo, F. Li, K. Xu, Y. Guo, Y. Liu, Z. Xia, J. Z Zhang, *J. Mater. Chem. C* **2019**, *7*, 2781.
[46] K. Ma, Y. Sheng, G. Wang, X. Zhang, Y. Di, C. Liu, L. Yu, L. Dong, Z. Gan, *J. Lumin.* **2022**, *243*, 118622.
[47] D. P. Nenon, K. Pressler, J. Kang, B. A. Koscher, J. H. Olshansky, W. T. Osowiecki, M. A. Koc, L.-W. Wang, A. P. Alivisatos, *J. Am. Chem. Soc.* **2018**, *140*, 17760.
[48] Y. Huang, W.-J. Yin, Y. He, *J. Phys. Chem. C* **2018**, *122*, 1345.
[49] Y. Li, C. Zhang, X. Zhang, D. Huang, Q. Shen, Y. Cheng, W. Huang, *Appl. Phys. Lett.* **2017**, *111*, 162106.
[50] J. Ye, M. M. Byranvand, C. O. Martínez, R. L. Z. Hoye, M. Saliba, L. Polavarapu, *Angew. Chem.* **2021**, *60*, 21636.
[51] X. Feng, Y. Sheng, K. Ma, F. Xing, C. Liu, X. Yang, H. Qian, S. Zhang, Y. Di, Y. Liu, Z. Gan, *J. Phys. Chem. Lett.* **2022**, *10*, 2200706.
[52] S. Mourdikoudis, M. Menelaou, N. Fiuza-Maneiro, G. Zheng, S. Wei, J. Pérez-Juste, L. Polavarapu, Z. Sofer, *Nanoscale Horiz.* **2022**, *7*, 941.
[53] X. Shen, K. Kang, Z. Yu, W. H. Jeong, H. Choi, S. H. Park, S. D. Stranks, H. J. Snaith, R. H. Friend, B. R. Lee, *Joule* **2023**, *7*, 272.
[54] L. Fei, L. Yang, P. Li, J. Ma, *Adv. Opt. Mater.* **2025**, *13*, 2402826.
[55] H. Choe, H. Jin, S. J. Lee, J. Cho, *Chem. Mater.* **2023**, *35*, 5401.
[56] N. Fiuza-Maneiro, K. Sun, I. López-Fernández, S. Gómez-Graña, P. Müller-Buschbaum, L. Polavarapu, *ACS Energy Lett.* **2023**, *8*, 1152.
[57] A. M. Ganose, D. O. Scanlon, A. Walsh, R. L. Z. Hoye, *Nature Commun.* **2022**, *13*, 4715.
[58] J. Kim, C.-H. Chung, K.-H. Hong, *Phys. Chem. Chem. Phys.* **2016**, *18*, 27143.
[59] M. Imran, P. Ijaz, L. Goldoni, D. Maggioni, U. Petralanda, M. Prato, G. Almeida, I. Infante, L. Manna, *ACS Energy Lett.* **2019**, *4*, 819.
[60] Y. Ding, Z. Zhang, S. Toso, I. Gushchina, V. Trepalin, K. Shi, J. W. Peng, M. Kuno, *J. Am. Chem. Soc.* **2023**, *145*, 6362.
[61] C. Otero-Martínez, N. Fiuza-Maneiro, L. Polavarapu, *ACS Appl. Mater. Inter* **2022**, *14*, 34291.
[62] Y. Ding, Z. Zhang, S. Toso, I. Gushchina, V. Trepalin, K. Shi, J. W. Peng, M. Kuno, *J. Am. Chem. Soc.* **2023**, *145*, 6362.
[63] V. Pinchetti, A. Anand, Q. A. Akkerman, D. Sciacca, M. Lorenzon, F. Meinardi, M. Fanciulli, L. Manna, S. Brovelli, *ACS Energy Lett.* **2018**, *4*, 85. .
[64] B. Luo, Y. Guo, X. Li, Y. Xiao, X. Huang, J. Z. Zhang, *J. Phys. Chem. C* **2019**, *123*, 14239.
[65] D. Ricciarelli, D. Meggiolaro, P. Belanzoni, A. A. Alothman, E. Mosconi, F. De Angelis, *ACS Energy Lett.* **2021**, *6*, 1869.
[66] S. Brinck, F. Zaccaria, I. Infante, *ACS Energy Lett.* **2019**, *4*, 2739.
[67] H. Li, X. Liu, D. Zhou, B. Dong, L. Xu, X. Bai, H. Song, *Adv. Mater.* **2023**, *35*, 2300118.
[68] A. Shukla, G. Kaur, K. J. Babu, A. Kaur, D. K. Yadav, H. N. Ghosh, *J. Phys. Chem. Lett.* **2022**, *13*, 83.

© 2025 The Author(s). Advanced Optical Materials published by Wiley-VCH GmbH